Charge disproportionation and the pressure-induced insulator–metal transition in cubic perovskite $PbCrO_3$

Jinguang Cheng[a,b,c], K. E. Kweon[d], S. A. Larregola[a], Yang Ding[e], Y. Shirako[a], L. G. Marshall[a,f], Z.-Y. Li[a], X. Li[a], António M. dos Santos[g], M. R. Suchomel[e], K. Matsubayashi[c], Y. Uwatoko[c], G. S. Hwang[d], John B. Goodenough[a,1], and J.-S. Zhou[a,1]

[a]Materials Science and Engineering Program and Texas Materials Institute, University of Texas at Austin, Austin, TX 78712; [b]Beijing National Laboratory for Condensed Matter Physics and Institute of Physics, Chinese Academy of Sciences, Beijing 100190, China; [c]Institute for Solid State Physics, University of Tokyo, Kashiwa 277-8581, Japan; [d]Chemical Engineering and Texas Materials Institute, University of Texas at Austin, Austin, TX 78712; [e]Advanced Photo Source, Argonne National Laboratory, Argonne, IL 60439; [f]Department of Chemical Engineering, Northeastern University, Boston, MA 02115; and [g]Quantum Condensed Matter Division, Oak Ridge National Laboratory, Oak Ridge, TN 37831

Contributed by John B. Goodenough, December 29, 2014 (sent for review May 8, 2014)

The perovskite $PbCrO_3$ is an antiferromagnetic insulator. However, the fundamental interactions leading to the insulating state in this single-valent perovskite are unclear. Moreover, the origin of the unprecedented volume drop observed at a modest pressure of P = 1.6 GPa remains an outstanding problem. We report a variety of in situ pressure measurements including electron transport properties, X-ray absorption spectrum, and crystal structure study by X-ray and neutron diffraction. These studies reveal key information leading to the elucidation of the physics behind the insulating state and the pressure-induced transition. We argue that a charge disproportionation $3Cr^{4+} \rightarrow 2Cr^{3+} + Cr^{6+}$ in association with the 6s-p hybridization on the Pb^{2+} is responsible for the insulating ground state of $PbCrO_3$ at ambient pressure and the charge disproportionation phase is suppressed under pressure to give rise to a metallic phase at high pressure. The model is well supported by density function theory plus the correlation energy U (DFT+U) calculations.

high pressure | perovskite | insulator–metal transition | charge disproportionation

Electron–electron correlations can open up a gap near the Fermi energy in a partially filled band system to give rise to a Mott insulator without changing the translation symmetry (1). However, how to justify the insulating ground state in the cubic perovskite $PbCrO_3$ with a 2/3-filled band remains controversial (2–11). An unphysically large U needs to be used in the density function theory (DFT) calculation (10) to open a gap, indicating that electron–electron correlations alone is insufficient to account for the insulator phase. More surprisingly, the structure undergoes a first-order transition at $P = 1.6$ GPa to another cubic phase with an extremely large volume drop (6). To clarify the fundamental interactions leading to the cubic insulating state and whether the pressure–induced volume collapse is accompanied with an insulator–metal transition, we carried out a suite of high-pressure experiments including structural characterization, measurements of resistivity, and X-ray absorption near edge structure (XANES) under high pressure and performed DFT with Hubbard U correction (DFT+U) calculations. Detailed information about the experiments, the DFT calculation, and the simulation for XANES is provided in *SI Text*.

The $PbCrO_3$ perovskite was known to be stabilized under high pressure and high temperature (HPHT) in the 1960s (2). Structural studies by X-ray and neutron diffraction revealed that it crystallizes as a cubic *Pm-3m* perovskite with a lattice constant of $a_0 \sim 4.00$ Å and exhibits a type G antiferromagnetic (AFM) order below $T_N = 240$ K in contrast to the type C AFM order of $CaCrO_3$ below $T_N = 90$ K and that of the tetragonal phase of $SrCrO_3$. The magnetic moment on Cr^{4+} as refined from neutron diffraction is 1.9 μ_B, which is very close to the spin-only moment of 2 μ_B expected for localized d^2 electrons. In comparison with other Cr^{4+}-containing perovskites, $ACrO_3$ (A = Ca, Sr) (9, 12), $PbCrO_3$ exhibits peculiar structural and physical properties. The unit-cell volume V_0 of $PbCrO_3$ is significantly larger than expected based on the A cation size r_A (13) in the $A^{2+}Cr^{4+}O_3$ family and the prediction with the software SPuDs (14). $PbCrO_3$ also shows a much higher resistivity and activation energy E_a than those found in $CaCrO_3$ and $SrCrO_3$ (9). These peculiarities of $PbCrO_3$ may be attributed to the sterochemical effect of the Pb $6s^2$ lone-pair electrons, but this effect normally reduces the symmetry from cubic. A comparative study of the electron energy loss spectroscopy (EELS) of $ACrO_3$ (A = Ca, Sr, Pb) perovskites by Arévalo-Lópe et al. (4) has indeed shown a subtle difference in the O-K edge spectra as a result of different A–O interactions. In the calculation by Ganesh and Cohen (7), the peculiar electronic configuration on Pb^{2+} makes Pb off-centering energetically favorable to form a tetragonal structure at ambient pressure as occurs in $PbTiO_3$. High pressure favors the cubic phase by suppressing the Pb off-centering displacement. However, the metallic phase predicted with this model does not match the experimental result for the phase at ambient condition. Moreover, a tetragonal phase is not confirmed by experiments.

Results and Discussion

In addition to an unusually large cell volume, $PbCrO_3$ is well known to have a highly irregular peak profile in the X-ray diffraction (XRD) pattern (3). This observation motivates us to

Significance

The steric activity of the lone pair electrons of Pb^{2+}-containing compounds distorts the crystal structure and produces exotic physical properties. In ferroelectric $PbTiO_3$ and $PbVO_3$, the lone-pair electrons hybridizing with the oxygen lead to polarized MO_6 octahedra. In $PbRuO_3$, the hybridization induces unprecedented Pb-Ru bonds at high pressure. The sterochemical effect in $PbCrO_3$ makes Pb bond with oxygen without a long-range periodicity. Under the influence of displaced Pb^{2+}, Cr^{4+} undergoes a charge disproportionation that opens up a gap. In contrast to the pressure effect on $PbTiO_3$ and $PbRuO_3$, pressure restores the undistorted perovskite structure in $PbCrO_3$. This result implies that the sterochemical effect of Pb^{2+} in a perovskite depends sensitively on the number and energy of the *d* electrons.

Author contributions: J.C., J.B.G., and J.-S.Z. designed research; J.C., K.E.K., S.A.L., Y.D., Y.S., L.G.M., Z.-Y.L., X.L., A.M.d.S., M.R.S., G.S.H., and J.-S.Z. performed research; K.M. and Y.U. contributed new reagents/analytic tools; K.E.K., S.A.L., Y.D., G.S.H., and J.-S.Z. analyzed data; and J.C., S.A.L., G.S.H., J.B.G., and J.-S.Z. wrote the paper.

The authors declare no conflict of interest.

[1]To whom correspondence may be addressed. Email: jgoodenough@mail.utexas.edu or jszhou@mail.utexas.edu.

This article contains supporting information online at www.pnas.org/lookup/suppl/doi:10.1073/pnas.1424431112/-/DCSupplemental.

refine the X-ray diffraction pattern with a structural model where Pb is at a general position. Whereas the refinement of the synchrotron X-ray diffraction (SXRD) pattern with a model allowing Pb displaced from the special position (1/2, 1/2, 1/2) to a general position (x, x, x) with x = 0.556 in the *Pm-3m* structure looks similar to as that with the regular structural model by Arevalo-Lopez et al. (3), see Fig. S1 for the refinement result with a full range of 2θ. A careful inspection of the refinement, particularly in the 2θ range of 13–19° (Fig. 1*A*) indicates that the match between the calculated profile and the experimental one is rather poor. As shown in Fig. 1*A*, the difference between the experimental and calculated profiles is positive for some peaks, whereas it is negative for the other peaks, although the reasonable reliability factors listed in Table S1 can still be achieved. In addition, the thermal factor B_{iso} at the Cr site extracted from the refinement of X-ray diffraction is unusually large. This observation suggests the presence of a static disorder of Cr atoms. To mimic a disordered sphere around the Cr (0,0,0) position, we allowed Cr at the general Wyckoff position 8g (x, x, x) with x = 0.035 in the refinement. The new structural model gave a significantly improved fitting quality. Both the overall intensity and the peak profile match well with the calculated values, and the B_{iso} at the Cr site is back to a normal value (see Table S1 for detailed results of structural refinements). Because XRD gives an averaged atomic position, the atomic disorder at the Cr sites yields different Cr–O bonds that should also be reflected in the oxygen thermal factor. Although neutron diffraction does not show convincing superlattice peaks for long-range ordering, the B_{iso} at the

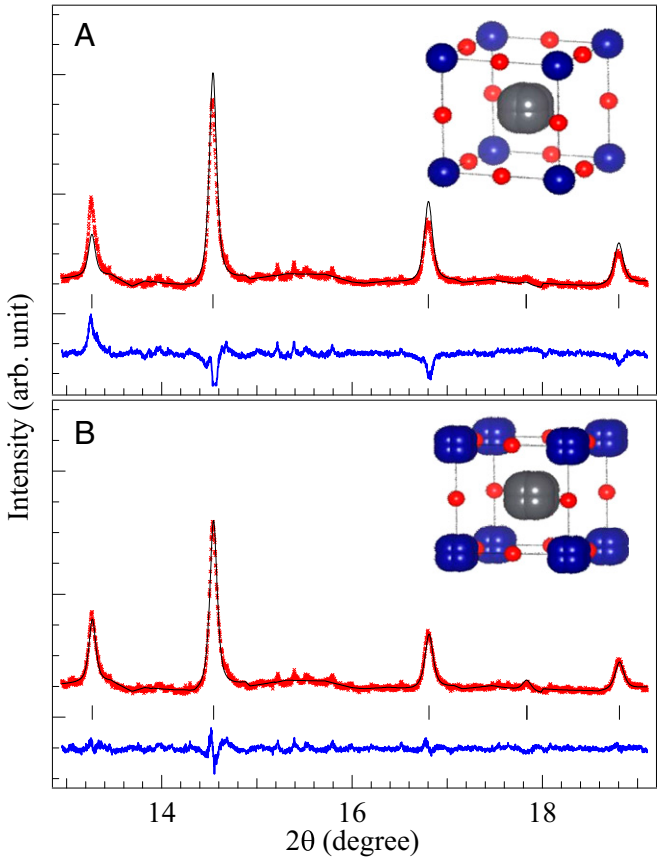

Fig. 1. Powder SXRD pattern of $PbCrO_3$ with the wave length λ = 0.41396 Å and results of the Rietveld refinement with (*A*) model of a cubic phase with Pb at the general position and the Cr thermal factor being fixed at 1 $Å^2$ and (*B*) model of a cubic phase with both Pb and Cr at general positions and thermal factors being refined (Table S1).

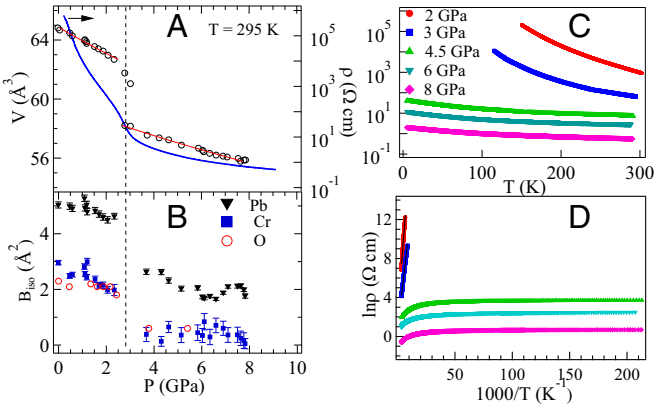

Fig. 2. (*A*) Pressure dependence of the unit-cell volume V(P) and resistivity ρ(P); solid lines inside the V(P) data are the fitting results to the BM equation (see *SI Text* for details of the BM equation). The fitting gave the bulk modulus $B_0 = 68 \pm 3$ GPa for the LP phase and 98 ± 3 for the HP phase. (*B*) Thermal factor B_{iso} at Pb, Cr, and O sites at room temperature for $PbCrO_3$ under different pressures. Thermal factors in this plot are from the refinements of neutron and laboratory X-ray diffraction patterns. The values at ambient pressure may not be as accurate as those obtained by the refinement of synchrotron diffraction (in Table S1). (*C*) Temperature dependence of resistivity ρ(T) under hydrostatic pressures up to 8 GPa. (*D*) Arrhenius plot of the ρ(T) data.

O position from the refinement is unusually large (2 A^2) compared with 0.2–0.44 A^2 found in other Cr^{4+}-containing perovskites (15). These observations are important clues for us to propose the charge disproportionation (CD) model for $PbCrO_3$ at ambient conditions, which will be further elaborated in the computational section below.

Fig. 2*A* shows the lattice parameter change under high pressure. An abrupt first-order phase transition can be clearly seen near 3 GPa. It should be noticed that the critical pressure P_c for the sample synthesized with a large volume press is higher than that reported with the sample made under a diamond anvil cell and laser heating (6). The same observation has been made by Wang et al. (11) in their transport measurement under pressure. Superimposed in the V-P curve of Fig. 2*A* is the result of the resistivity change under pressure. It is clear that the first-order structural transition is accompanied by a drop in the resistivity of more than two orders of magnitude. The resistivity change on crossing the transition is much more obvious than that reported by Wang et al. (11). We further measured the temperature dependence of resistivity under different pressures. As shown in Fig. 2 *C* and *D*, ρ(T) of $PbCrO_3$ at $P < P_c$ is very large and activated, which is consistent with a large thermoelectric power of S ~ 300 μV/K obtained near room temperature for an insulator. The perovskite $PbCrO_3$ becomes a conductor at $P > P_c$; the temperature-independent ρ(T) and slight up-turn at low temperatures appear to be caused by grain-boundary scattering in the metallic phase of the polycrystalline sample. The structural study under high pressure with a laboratory X-ray source is incapable of providing detailed information about the profile change of diffraction peaks on crossing the phase transition, and as such, the simple structural model with Pb and Cr at their special sites was used in the refinement. Similar to the result of refining the SXRD data with the simple cubic model, B_{iso} at both Pb and Cr sites is large for the phase at ambient pressure and up to P_c ~ 3 GPa. The in situ neutron diffraction is critical to monitor the change at the oxygen position on crossing the pressure-induced transition. The B_{iso} for the phase at ambient pressure is unusually large. Discontinuous drops of B_{iso} for Pb, Cr, and O on crossing P_c reflect that the cation disorder in the low-pressure phase is suppressed on crossing P_c, which is consistent with a transition from the CD phase to a metal.

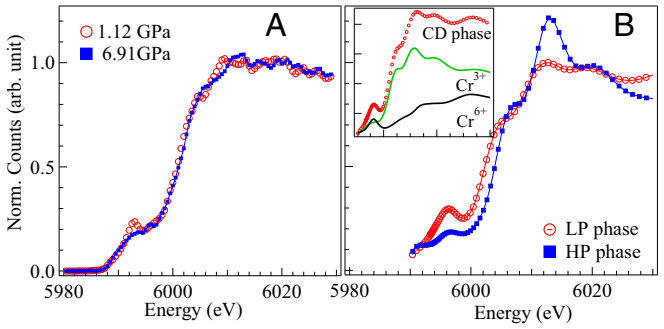

Fig. 3. (*A*) The XANES data of $PbCrO_3$ under two pressures, one on each side of P_c. (*B*) Calculated XANES with the CD model for the LP phase and the simple cubic structure for the HP phase. *Inset* in *B* shows contributions from Cr^{3+} and Cr^{6+} in the XANES calculation for the CD model.

In addition to measuring bulk properties of $PbCrO_3$ under pressure, we used Cr Kα PYF XANES as a microscopic probe to investigate directly the electronic structure change on crossing the transition. The PYF XANES of the Cr–K edge was collected at 1.12 and 6.91 GPa and is displayed in Fig. 3*A*. The pre-edge feature reflects the information of the empty 3*d* band structure above the Fermi energy, whereas the feature at the shoulder of the spectrum is mainly related to the empty Cr 4p band. The most obvious change between the low-pressure (LP) phase and the high-pressure (HP) phase is a diminishing of the hump at the pre-edge in the HP phase. Our calculations below explain well these changes in XANES by the insulator-metal transition and the structural change.

In the second half of this paper, we report our DFT+U calculations. In the HP cubic phase (*Pm-3m*), each Cr^{4+} ion must be located at an octahedral site with six equivalent Cr–O bonds, as required by the space group in Fig. 4*A*. Fig. 4*B* shows the electron density of states (DOSs) projected on the atomic orbitals of $PbCrO_3$; the threefold-degenerate Cr t_{2g} states are partially filled with two electrons, whereas the doubly degenerated Cr e_g states are completely empty. For U_{eff} = 2.13 eV used in our calculations, a clear exchange splitting means that a ferromagnetic state is more stable than an antiferromagnetic state*; the energy difference between the ferromagnetic and antiferromagnetic states is directly related to the U_{eff} value. A 1/3-filled metallic band is near the crossover from ferromagnetic coupling for a 1/4-filled band and antiferromagnetic ordering for a half-filled band. A metallic state as indicated by the band structure from our DFT calculations is consistent with experimental results. Our generalized gradient approximation (GGA)+U calculations also predict the lattice constant a and the bulk modulus B_0 to be 3.906 Å and 162.6 GPa, respectively, in agreement with the experimental values of a = 3.862 Å and B_0 = 187 GPa by Xiao et al. (6) The slight overestimation of a is due to the well-known underbinding tendency in the GGA calculation. A smaller $B_0 = 98 \pm 3$ GPa from the Birch-Murnaghan (BM) fitting in Fig. 2*A* can be attributed to a relatively narrow pressure range for this fit.

Now we turn to the cubic phase of $PbCrO_3$ at ambient pressure. Following the experimental observation, we first let the cell volume expand by 10% based on the HP cubic phase and search for local structural configurations with lower energy. We found that the cell volume expansion leads to significant atomic displacements from the ideal cubic positions; Cr^{4+} tends to undergo a charge disproportionation to $Cr^{+(4+\delta)}$ and $Cr^{+(4-\delta)}$. For a quantitative description of the CD phase, we constructed two model systems that consist of two and three $PbCrO_3$ formula units (f.u.), which can allow the $2 \times 4^+ \rightarrow 3^+ + 5^+$ and $3 \times 4^+ \rightarrow 3^+ + 3^+ + 6^+$. As illustrated in Fig. 5*A*, the equilibrium volume for the CD configuration $3^+ + 3^+ + 6^+$ is predicted to be 65.2 $Å^3$/f.u., which is about 9% greater than 59.6 $Å^3$/f.u. for the HP cubic structure. The bulk modulus B_0 for the CD phase is calculated to be 78.2 GPa, which is close to the experimental value $B_0 = 68 \pm 3$ GPa in Fig. 2*A*. On the other hand, the $3^+ + 5^+$ configuration tends to be rather unstable and thus returns to the HP cubic structure on volume relaxation. However, we should point out that the energy difference between the $3^+ + 5^+$ and $3^+ + 3^+ + 6^+$ model structures is insignificant (~ 0.06 eV/f.u. at a fixed volume of 64.7 $Å^3$); this may imply that, at elevated temperatures, Cr^{5+} would possibly coexist with prevailing Cr^{3+} and Cr^{6+}.

In an optimized model structure with the $3^+ + 3^+ + 6^+$ configuration shown in Fig. 5*B*, Pb atoms are displaced substantially toward Cr^{3+} atoms (which also deviate slightly from the ideal cubic positions). The average displacements of Pb and Cr atoms with respect to the cubic lattice are predicted to be 0.37 and 0.20 Å, respectively; those displacements could provide an explanation for the observed irregular profile of the XRD peaks. The Cr^{3+} and Cr^{6+} are found to be octahedrally and tetrahedrally coordinated, respectively, by O anions, yielding CrO_6 octahedra and highly distorted CrO_4 tetrahedra by random displacements of the Cr^{6+} within an octahedral site as indicated in Fig. 5*B*. In a distorted CrO_4 tetrahedron, there are two short Cr–O bonds (with double bond Cr=O character) and two relatively long bonds (with single bond Cr–O character); the respective bond distances of 1.65 and 1.78 Å are comparable to 1.59 and 1.78 Å for the calculated Cr=O and Cr–O bonds in a tetrahedral $CrO_2(OH)_2$ cluster in the gas phase. In neighboring Cr^{6+} and Cr^{3+} octahedra, a bridging O anion tends to move toward neighboring Cr^{6+} to give a long Cr–O bond distance of 2.40 Å, whereas the other five Cr–O bonds have bond lengths of 2.00 ± 0.05 Å, which is close to a typical Cr^{3+}–O bond distance of 2.0 Å in $RCrO_3$ (16). It is also worthwhile to note that the distance from Pb atoms to O atoms (connected to Cr^{3+} atoms) is 2.43–2.56 Å, which is substantially shorter than the 2.85 Å estimated for the ideal cubic case; the shorter Pb–O bonds are indicative of a possible contribution of the Pb-O interaction to stabilizing the CD phase (*vide infra*).

As shown in Fig. 5*C*, the DOS analysis for the ambient-pressure phase of $PbCrO_3$ with the $3^+ + 3^+ + 6^+$ configuration clearly demonstrates that the charge disproportionation provokes an energy gap in the Cr^{5+}/Cr^{4+} redox band, in contrast to the ideal cubic structure of Fig. 4. The upper valence bands from 0 eV down to −1.2 eV consist mainly of half-filled Cr^{3+} t_{2g} and O 2*p* orbitals, whereas the empty t_{2g} orbitals of Cr^{6+} primarily constitute the conduction band minimum. The DOS plot also shows

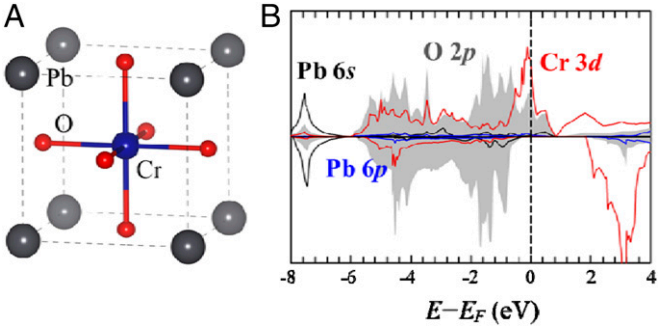

Fig. 4. (*A*) Schematic drawing of a cubic perovskite structure at $P > P_c$. (*B*) DOS projected on the atomic orbitals of the HP $PbCrO_3$ phase; the dash line indicates the position of the Fermi level.

*The relative stability tends to be sensitive to the choice of Ueff; nonetheless, both the ferromagnetic and antiferromagnetic states are predicted to be metallic, which is consistent with experiments.

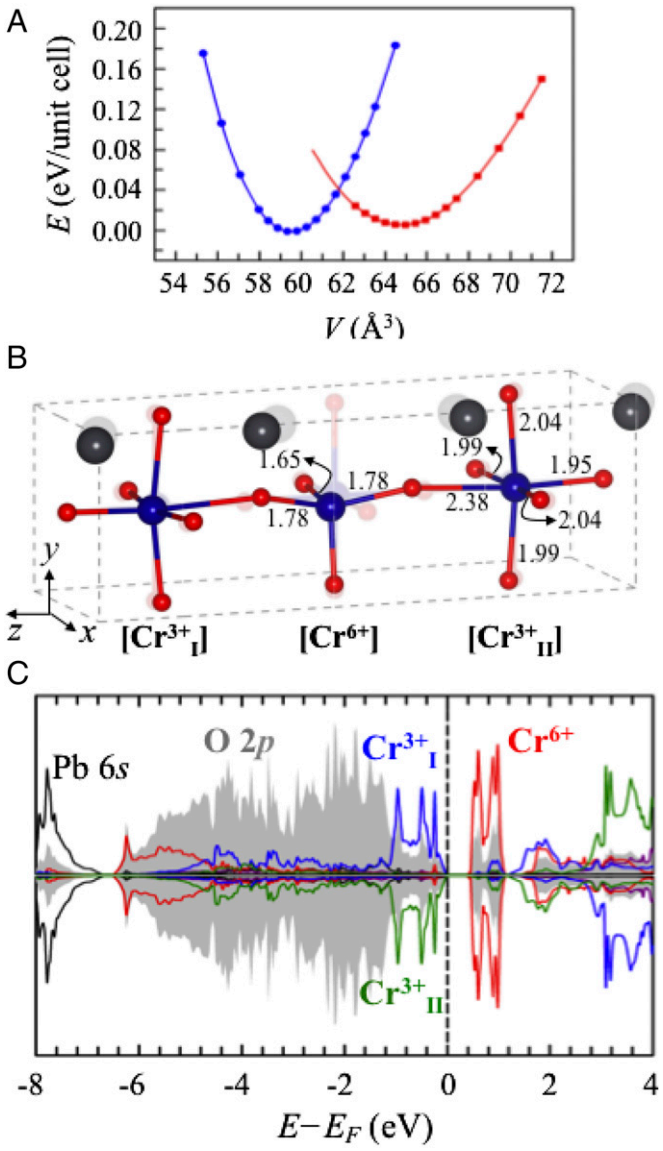

Fig. 5. (*A*) The relative energies (*E*) per formula unit (f.u.) for the ideal cubic perovskite (blue) and the CD (red) phases of $PbCrO_3$ as a function of cell volume (*V*). (*B*) The optimized CD model structure with bond length in Angstroms together with the ideal cubic structure shown as faded structure at the background. (*C*) DOS projected on the Pb6s, O2p, and Cr3d orbitals in the CD model.

that two adjacent Cr^{3+} ions have an overlapping half-filled t^3 orbital to give an antiferromagnetic coupling, which is consistent with the rules for superexchange interactions and the type-G AF ordering observed. The overlap of the Pb *6s,6p* and Cr *3d* energies in the range $E_f - 4.5$ eV $< E < E_f - 1.2$ eV indicates the existence of strong interactions that are manifest as empty antibonding primarily Cr^{6+}:*3d* states and filled bonding Pb *6s,6p*. The Pb–O interactions stabilize the localized Cr^{3+}:t^3 states via the inductive effect to create an energy gap between Cr^{6+} and Cr^{3+} *3d* states. To confirm the role of Pb in the electronic structure of $PbCrO_3$, we also performed the same calculation for isostructural $SrCrO_3$. The CD phase with the $3^+ + 3^+ + 6^+$ configuration having half-filled and empty t_{2g} states turns out to be highly unlikely; instead the phase with partially filled Cr t_{2g} orbitals is more stable (Fig. S2). The predicted cubic phase for $SrCrO_3$ is consistent with the experimental result. Additionally, we also found that the Cr t_{2g} orbitals become partially filled instead of fully empty or half-filled where the Pb–O interaction is reduced by moving Pb atoms back to the ideal cubic positions (Fig. S3). This analysis highlights that the peculiar electron configuration on Pb and its nuclear position shifting from the position in the ideal cubic structure play important roles in the charge disproportionation of Cr in $PbCrO_3$ at ambient pressure.

Finally, XANES data provide an important test to our CD model and our picture of the pressure-induced insulator–metal transition. The shape and position of the Cr *K*-edge are well known to be a strong function of Cr valence (17–19). As displayed in Fig. 3*A*, one distinct difference between the two measured XANES spectra is that the LP $PbCrO_3$ phase exhibits a single intense pre-edge peak, whereas the intensity of the pre-edge peak is significantly reduced for the HP phase. As shown in Fig. 3*B*, the calculated XANES for the CD and the simple cubic phases captures the essential features of the experimental results. The strong absorption peak in the pre-edge region is generally attributed to a quadruple transition of a 1*s* electron to an empty antibonding 3d t_{2g}. (20) As shown in a decomposed plot of the calculated XANES in the *Inset* of Fig. 3*B*, the pre-edge peak is primarily due to the contribution from Cr^{6+}. However, the same transition is not allowed in a high-symmetry octahedral environment of Cr^{6+} or Cr^{4+} (17–19). It should be stressed that the pattern given in Fig. 5*B* is one of possible CD of $PbCrO_3$ at ambient pressure.

Summary of Experimental Findings and the DFT Calculation

A combination of new experiments and DFT+U calculations allows us to clarify the nature of the insulator phase and the mechanism of the pressure-induced first-order transition in perovskite $PbCrO_3$. In contrast to $PbVO_3$ in which shortening the distance between Pb^{2+} and V^{4+} to share the lone-pair electrons leads to a tetragonal polar phase, the Pb displacements in $PbCrO_3$ are distributed around its position in the cubic perovskite structure. Assisted by static disordered Pb-O bonding, a negative-U charge density wave on Cr–O arrays provides an inelastic energy that competes with the electron–electron correlation to give rise to the insulator phase at ambient pressure. The simulated XANES profile based on the charge disproportionation model matches well the experimental data. The cell-volume collapse at $P_c \sim 3$ GPa is due to a first-order localized to itinerant electronic transition as demonstrated by our transport property and XANES under high pressure. The lattice parameter, bulk modulus, and the result of XANES measurement of the metallic phase at high pressure can be well-described by our DFT+U calculations. The predicted ferromagnetic phase at $P > P_c$ remains to be confirmed by experiment.

Materials and Methods

Polycrystalline $PbCrO_3$ samples used in the present study were obtained by sintering a stoichiometric mixture of PbO and CrO_2 powders at 8 GPa and 800 °C for 30 min with a Walker-type multianvil module. High-resolution diffraction data (SXRD) have been collected in the temperature range of 120–300 K with synchrotron radiation on beamline 11-BM ($\lambda = 0.41396$ Å) at the Advanced Photon Source, Argonne National Laboratory. The obtained SXRD data were analyzed with the Rietveld method by using the General Structure Analysis System (GSAS) program. The high-pressure structural study at room temperature was carried out with a diamond-anvil cell mounted on a four-circle diffractometer with Mo anode. In situ high-pressure neutron diffraction measurements were measured at the SNAP beamline in the Spallation Neutron Source in Oak Ridge National Laboratory. The SNAP instrument is a medium resolution time of flight diffractometer optimized for measurements under high pressure. Temperature dependence of resistivity down to 4.5 K under different hydrostatic pressures up to 8 GPa was measured with the four-probe method in a cubic anvil apparatus. The Cr Kα partial fluorescence yield (PFY) X-ray absorption spectrum under pressure was collected at HPCAT-16IDD, Advance Photon Sources of Argonne National Laboratory, using a Panoramic diamond anvil cell.

All calculations reported herein were performed by using DFT with Hubbard U correction (DFT+U) within the GGA-PBE, as implemented in the Vienna Ab-initio Simulation Package (VASP 5.2.2).

Note Added in Proof. While this paper was in press, we have become aware of a report by Wu, et al. (21). The authors have studied the X-ray absorption spectra of $PbCrO_3$ under pressure; they have reached a similar conclusion that a charge disproportionation occurs in the low-pressure phase of $PbCrO_3$.

ACKNOWLEDGMENTS. The Texas Advanced Computing Center is acknowledged for providing HPC resources. This work was supported by the National Science Foundation (NSF) Materials Interdisciplinary Research Teams (Division of Material Research-1122603) and the Welch Foundation (F-1066 and F-1535). J.C. acknowledges the support of the Strategic Priority Research Program of the Chinese Academy of Sciences (Grant XDB07000000), the Ministry of Science and Technology (MOST) and NSF of China (Grants 2014CB921500 and 11304371), and Japan Society for the Promotion of Science (JSPS) fellowship for foreign researchers (Grant 12F02023). Use of the Advanced Photon Source at Argonne National Laboratory was supported by the US Department of Energy, Office of Science, Office of Basic Energy Sciences, under Contract DE-AC02-06CH11357. Research at Spallation Neutron Source in Oak Ridge National Laboratory was sponsored by the Scientific User Facilities Division, Office of Basic Energy Sciences, US Department of Energy.

1. Mott NF (1949) The basis of the electron theory of metals, with special references to the transition metals. *Proc Phys Soc London Sect A* 62(7):416–422.
2. Roth WL, DeVeies RC (1967) Crystal and magnetic strucutre of $PbCrO_3$. *J Appl Phys* 38(3):951–952.
3. Arevalo-Lopez AM, Alario-Franco MA (2007) On the structure and microstructure of $PbCrO_3$. *J Solid State Chem* 180(11):3271–3279.
4. Arevalo-Lopez AM, Castillo-Martinez E, Alario-Franco MA (2008) Electron energy loss spectroscopy in $ACrO_3$ A=Ca, Sr and Pb perovskites. *J Phys Condens Matter* 20(50):505207.
5. Arévalo-López AM, Dos santos-García AJ, Alario-Franco MA (2009) Antiferromagnetism and spin reorientation in "PbCrO3". *Inorg Chem* 48(12):5434–5438.
6. Xiao W, Tan D, Xiong X, Liu J, Xu J (2010) Large volume collapse observed in the phase transition in cubic $PbCrO_3$ perovskite. *Proc Natl Acad Sci USA* 107(32):14026–14029.
7. Ganesh P, Cohen RE (2011) Orbital ordering, ferroelasticity and the large pressure-indcued volume collapse in $PbCrO_3$. *Phys Rev B* 83(17):172102.
8. Wang BT, Yin W, Li WD, Wang F (2012) First-principles study of the pressure-induced phase transition and electronic property of $PbCrO_3$. *J Appl Phys* 111(1):013503.
9. Komarek AC, et al. (2011) Magnetc order, transport, and infrared optical properties in the $ACrO_3$ system A=Ca, Sr, and Pb. *Phys Rev B* 84(12):125114.
10. Lu Y, He D, Peng F, Cheng X (2013) The mystery of abnormally large volume of $PbCrO_3$ with a structurally consistent Hubbard U from first-principles. *Eur Phys J B* 86(8):352.
11. Wang WD, He DW, Xiao WS, Wang SM, Xu JA (2013) Electrical characterization in the phase transition between cubic $PbCrO_3$ Perovskites at high pressures. *Chin Phys Lett* 30(11):117201.
12. Zhou J-S, Jin C-Q, Long Y-W, Yang L-X, Goodenough JB (2006) Anomalous electronic state in CaCrO3 and SrCrO3. *Phys Rev Lett* 96(4):046408.
13. Shannon RD (1976) Revised effective ionic radii and systematic studies of interatomic distance in halides and chalcogenides. *Acta Crystallogr A* 32(5):751–767.
14. Lufaso MW, Woodward PM (2001) Prediction of the crystal structures of perovskites using the software program SPuDS. *Acta Crystallogr B* 57(Pt 6):725–738.
15. Castillo-Martinez E, Duran A, Alario-Franco MA (2008) Structure, microstructure and magnetic properties of $Sr_{1-x}Ca_xCrO_3$ ($0 < x < 1$). *J Solid State Chem* 181(4):895–904.
16. Zhou J-S, et al. (2010) Intrinsic structural distortion and superexchange interaction in the orthrohombic rare-earth perovskite $RCrO_3$. *Phys Rev B* 81(21):214115.
17. Arcon I, Mirtic B, Kodre A (1998) Determination of valence states of chromium in calcium chromates by using X-ray absorption near-edge structure (XANES) spectroscopy. *J Am Ceram Soc* 81(1):222.
18. Pantelouris A, Modrow H, Pantelouris M, Hormes J, Reinen D (2004) The influence of coordination geometry and valency on the K-edge absorption near edge spectra of selected chromium compounds. *Chem Phys* 300(1-3):13–22.
19. Qiao L, et al. (2013) The impact of crystal symmetry on the electronic structure and functional properties of complex lanthanum chromium oxides. *J Mater Chem C* 1(30): 4527–4535.
20. Joseph D, Yadav AK, Jha SN, Bhattacharyya D (2013) Chemical shift of Mn and Cr K-edges in X-ray absorption spectroscopy with synthrotron radiation. *Bull Mater Sci* 36(6):1067–1072.
21. Wu M, et al. (2014) Pressure-induced valence change and semiconductor-metal transition in $PbCrO_3$. *J Phys Chem* 118(40):23274–23278.